Chapter 16
The Nonlinear Restoring Force Method: An Overview with Numerical and Experimental Applications

Cristiano Martinelli and Andrea Cammarano

Abstract The stringent CO2 policies and the competitive market are increasing the demand for lightweight high-performance structures in many engineering sectors. Under normal operations, these structures may experience large deformations which may lead the dynamics of the systems into the nonlinear regime. Consequently, methods and approaches for the analysis and the identification of accurate mathematical models, capable of representing the dynamics of such systems, have become of central importance in the current scientific research. This paper proposes an overview of a novel approach for the identification of strongly nonlinear systems, named the Nonlinear Restoring Force (NLRF) method. Based on the classical Restoring Force Surface (RFS) method, this approach separates the nonlinear contribution of the restoring force from the linear one exploiting well-established linear identification methods currently used in industrial practices. This enables the visualisation of the pure nonlinear part of the restoring force surface, facilitating the identification of an appropriate mathematical function capable of capturing the nonlinear behaviour of the system. Firstly the mathematical background of the theory and numerical examples are presented and then, to show the capabilities of the method, nonlinear Reduced Order Models are identified from experimental data. To this end, the dynamics of two experimental test rigs, characterised by geometric (smooth) and localised (non-smooth) nonlinearities, are presented and analysed. Finally, all the identified models are validated against experimental data, using different excitation levels to test their prediction accuracy.

Keywords Nonlinear System Identification· Nonlinear Dynamics· Model Updating· Experimental Analysis· FEA

Introduction

Lightweight high-performance structures are becoming popular in many engineering sectors. The advantages of these structures consist in using less material and obtaining a lightweight structure. Historically the space sector has been interested in reduce the weight of systems, as the cost of space mission is directly proportional to the weight, a good cost predictor [1]. Nonetheless, in recent years, other engineering sectors such as the civil, power, and transport industries [2] have also developed an interest in lightweight structures. This interest is driven by the stringent CO2 policies [3, 4] which force industries to reduce their emissions. Despite these advantages, lightweight structures are characterised by slender sections which can induce the nonlinear dynamic responses when large deformations are achieved.

Nowadays, the identification of linear models via model updating procedures [5] and modal experimental analysis of linear structures [6] are considered well-established practices by the scientific and industrial engineering community. On the contrary, a solid and robust procedure for the identification of nonlinear mechanical systems has not been developed yet, but rather several methods have been proposed. Kerschen, Noël and collaborators [7, 8] provided a systematic review of the different methods for the identification of nonlinear systems: between the different methods, the Restoring Force Surface (RFS) method [9] is considered one of the most well-established identification methods for nonlinear systems. The RFS method has been successfully used for the identification of several nonlinear systems from experimental data: for example, Bonisoli and Vigliani [10] adopted the RFS method to identify the nonlinear parameters of a passive magneto-elastic suspension,

Cristiano Martinelli · Andrea Cammarano
Department of Aeronautical and Astronautical Engineering, University of Southampton, U.K.
e-mail: c.martinelli@soton.ac.uk

Andrea Cammarano
James Watt School of Engineering, University of Glasgow, U.K.
e-mail: A.Cammarano@soton.ac.uk

Ludovic Renson et al. (eds.), *Nonlinear Structures & Systems, Vol. 1*, Conference Proceedings
of the Society for Experimental Mechanics Series, https://doi.org/10.13052/97887-438-0146-7_16

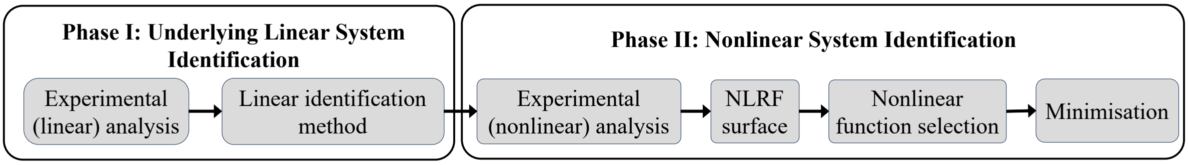

Fig. 1 Nonlinear Restoring Force (NLRF) method: outline of the procedure for the identification of nonlinear models.

Cammarano et al. [11] utilised the RFS method to obtain the nonlinear properties associated to a bistable mechanical system for vibration energy harvesting, and Kerschen et al. [12, 13] adopted the same method to identify a trilinear characteristics of a small real satellite and the nonlinear characteristics between the aircraft wings and fuel tanks.

Although efficient, the classical RFS method allows for the graphical representation of the restoring surface only when single Degree of Freedom (DOFs) systems are representative of the system dynamics and becomes computationally expensive when MDOF structures are considered [14]. This results in a difficult implementation of the method in the current industrial practices which rely on definition of MDOF linear models. To solve these problems, a modified version of the RFS method has been recently proposed by Martinelli et al. [15, 16], named the Nonlinear Restoring Force (NLRF) method. The method is build on existing linear identification methods and aims to identify the linear and nonlinear behaviour of the mechanical structure in a separate way. This allows the method to be easily implemented in the current industrial practices, facilitating the identification of nonlinear mechanical systems and structures. This paper proposes an overview of NLRF method: firstly the methodology is presented, then a numerical example is introduced to show how the method can be applied in practice. The method is then utilised to identify the nonlinear Reduced-Order Models (ROMs) of two experimental test rigs characterised by smooth and non-smooth nonlinearities. Finally, the identified nonlinear models are validated against experimental data that were not used during the identification phase.

Methodology, Background Theory, and Limitations

The methodology of the Nonlinear Restoring Force Surface Method is schematically described by Fig. 1. The procedure is divided into two different phases: in the first phase the underlying linear behaviour the system is identified while in the second phase aims to identify the nonlinear characteristics of the system. The linear behaviour of the system is identified using classical identification methods, such as Half Power method, Circle Fitting Method, or stabilisation diagram. During this phase, experimental linear analysis is performed by applying low amplitude random excitation to the structure. This excitation reduces the effect of smooth nonlinearities, e.g. hardening or softening stiffness, and allows estimating the underlying linear behaviour of the system [6, 17]. At this stage, a linear model representing the underlying linear behaviour of the system is identified using one of the aforementioned techniques and by selecting an appropriate number DOFs. In the second phase, the nonlinear dynamic behaviour of the system is identified. Firstly a nonlinear experimental analysis is performed; this often involves the usage of sinusoidal excitation at specific frequencies or forward/backward frequency sweeps to excite the nonlinear response of the structure. Then, the knowledge of underlying linear system and the experimental nonlinear data are utilised to obtain the nonlinear restoring force using the following expression:

$$\mathbf{NRF} = \mathbf{N}(\dot{\mathbf{x}}, \mathbf{x}) = \mathbf{F} - \mathbf{M}\ddot{\mathbf{x}} - \mathbf{C}\dot{\mathbf{x}} - \mathbf{K}\mathbf{x} \tag{1}$$

where $\mathbf{x} \in \mathbb{R}^{n\times 1}$ represents the displacement vector, $\mathbf{M}$, $\mathbf{C}$, and $\mathbf{K} \in \mathbb{R}^{n\times n}$, denote the linear mass, damping, and stiffness matrices, and $\mathbf{N}(\dot{\mathbf{x}}, \mathbf{x})$ and $\mathbf{F} \in \mathbb{R}^{n\times 1}$ are the nonlinear contribution and the forcing function. Eq. 1 results in a vector of nonlinear restoring forces for each DOF of the selected ROM. These restoring forces can be plotted in a sub-space of coordinate to obtain additional information about the nonlinear behaviour of the system. Specifically the visualisation of the nonlinear restoring force surface allows to:

- Understand if the selected sub-space of coordinates is sufficient to fully describe the nonlinear dynamics of the system [15].
- Identify and characterise localised nonlinearities [16].

These two features provide additional insights about the dynamics of the system and helps to define a suitable nonlinear function, e.g. a polynomial, for the identification of the nonlinear characteristics. An overview of the features is reported in Section Experimental Validation: Identification of Smooth and Non-Smooth Nonlinearities where the nonlinear dynamic behaviour of two experimental test rigs is identified using the proposed method: in the identification of the first test rig (characterised by only smooth nonlinearities), the NLRF method is utilised to understand if the nonlinear characteristics of each DOF of the structure can be fully described using only a sub-set of local coordinates, e.g. to understand if the nonlinear characteristic associated to the first DOF of the structure can be represented using a function of the type $N(x_1, \dot{x}_1)$. The second test rig is instead used to show how the proposed method can be used to identify localised nonlinearities.

One of the limitation of the proposed approach is the need of identifying an underlying linear system: to this end the considered mechanical system must behaves linearly at low amplitude of excitation. Without this feature, the method cannot be applied as the first phase of the procedure would be invalidated. Another limitation of the approach comes from the linear identification methods [6] and consists in the selection of an appropriate linear ROM: by selecting a ROM which does not capture the full dynamics of the system, the identification of the linear behaviour is inaccurate, and this affect the capability of the method in identifying the sought nonlinear characteristics.

Numerical Example: A Three Storey Building with a Localised Nonlinearity

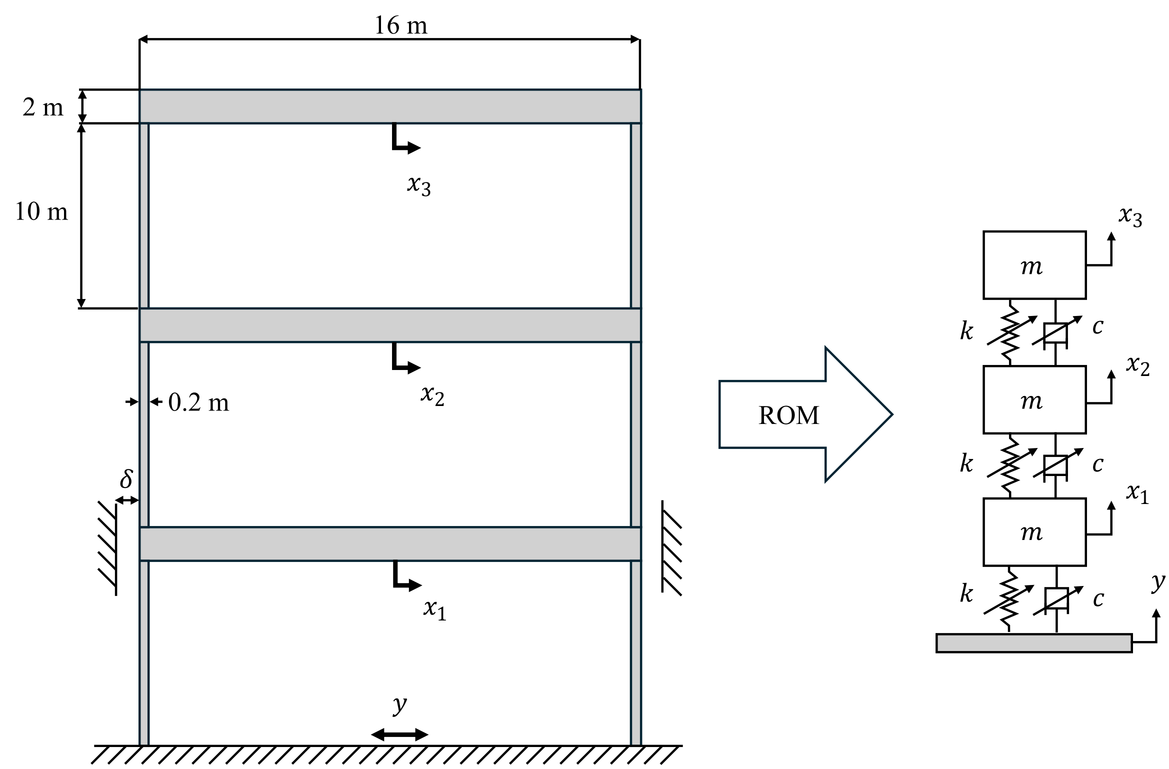

Fig. 2 Schematic representation of three storey building and the associated ROM.

A model of a building is considered as numerical example. The building is made in steel (elastic modulus $E = 210$ GPa, Poisson coefficient $\nu = 0.34$, and density $\gamma = 8000$ Kg/m^3) and has three storeys whose dimensions are described by Fig 2. The dynamics of the building is simulated using a FE model developed in ANSYS using plate element (PLANE42) to model each storey and beam elements (BEAM3) to model structural connection between each storey. The building is excited by the transversal excitation of the ground and a symmetric motion constraints at the first floor is applied to simulate the presence of a nonlinear characteristic. The nonlinear constraint is simulated in ANSYS by using the element COMBIN39 and by imposing a piecewise characteristic of the form:

$$F_p = \begin{cases} k_p(x_1 - \delta) & \text{if } x_1 > \delta \\ 0 & \text{if } -\delta < x_1 < \delta \\ k_p(x_1 + \delta) & \text{if } x_1 < -\delta \end{cases} \tag{2}$$

where δ denotes the semi non-contact gap and k_p the piecewise stiffness. Fig. 2 shows the ROM representing the three storey building: each floor shares the same dimensions and material therefore the stiffness (k), the damping (c), and the mass (m)

of each DOF of the ROM are considered to be the same. The final ROM results in the following equation of motion:

$$m\ddot{x}_1 + c(\dot{x}_1 - \dot{y}) + k(x_1 - y) - c(\dot{x}_2 - \dot{x}_1) - k(x_2 - x_1) + N_1(x,y) = 0 \tag{3a}$$
$$m\ddot{x}_2 + c(\dot{x}_2 - \dot{x}_1) + k(x_2 - x_1) - c(\dot{x}_3 - \dot{x}_2) - k(x_3 - x_2) + N_2(x,y) = 0 \tag{3b}$$
$$m\ddot{x}_3 + c(\dot{x}_3 - \dot{x}_2) + k(x_3 - x_2) + N_3(x,y) = 0 \tag{3c}$$

where $N_k(x,y)$ indicate a general nonlinear terms applied to the k-th DOF.

Linear and nonlinear FE simulations are performed to identify the underlying linear and nonlinear behaviour of the three storey building in time and frequency domain. The modal analysis shows that the first three natural frequencies are found at the following frequencies: 0.234 Hz, 0.657 Hz, 0.951 Hz. The cumulative mass fraction of these three modes displace more than 99% of the mass of the system (considering the first 20 modes). This analysis confirms that a 3 DOFs reduced-model is sufficient to describe the dynamics of the of the building. The Frequency Response Functions (FRFs) of the system are obtain via harmonic analysis: a based displacement Y of 0.01 m is imposed to the base of the model and the response of the system is measured at nodes located in the middle of each floor. The mass m of each floor is estimated by knowing the volume and the density of the material [1]. The stiffness k, instead, is obtained from the value of the natural frequencies which can be estimated via classical experimental modal analysis [6]. The value of the stiffness k is the obtained by solving $\omega_n = f(k)$ where $f(k)$ is obtained by solving the eigenvalues problem associated to the ROM. For the considered problem, the value of the natural frequencies are found:

$$\omega_{n,1} = 0.445\sqrt{k/m} \tag{4a}$$
$$\omega_{n,2} = 1.247\sqrt{k/m} \tag{4b}$$
$$\omega_{n,3} = 1.802\sqrt{k/m} \tag{4c}$$

Using Eq. 4 it is possible to obtain a value of the stiffness $k = 2.925e+06$ N/m by averaging the obtained results. Assuming a Rayleight proportional damping ($\alpha = 0$ and $\beta = 0.01$) for the FE simulations, the FRF of the model can be computed and used to identity a suitable damping factor c via iterative procedure. A final value of $c = 2.925e+04$ Ns/m is identified. At this point, it is possible to compare the FRF of the FE model and the identified ROM: the comparison is reported in Fig. 3 and shows that the reduced-model is able to reproduce the dynamic behaviour of the full model for the first three modes. Using the knowledge of the identified underlying linear model, it is possible to compute the nonlinear restoring forces for each DOF as follows:

$$NLF_1 = -m\ddot{x}_1 - c(\dot{x}_1 - \dot{y}) - k(x_1 - y) + c(\dot{x}_2 - \dot{x}_1) + k(x_2 - x_1) \tag{5a}$$
$$NLF_2 = -m\ddot{x}_2 - c(\dot{x}_2 - \dot{x}_1) - k(x_2 - x_1) + c(\dot{x}_3 - \dot{x}_2) + k(x_3 - x_2) \tag{5b}$$
$$NLF_3 = -m\ddot{x}_3 - c(\dot{x}_3 - \dot{x}_2) - k(x_3 - x_2) \tag{5c}$$

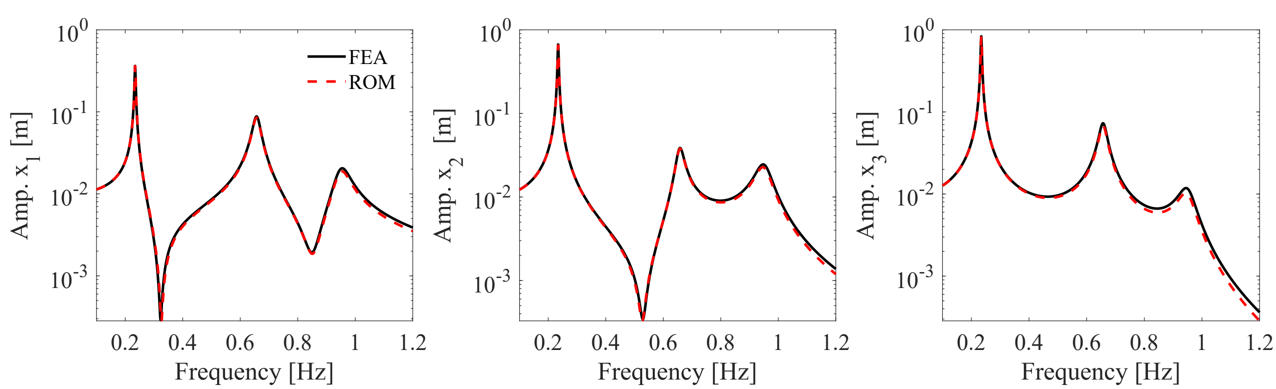

Fig. 3 Comparison between linear Frequency Response Functions (FRF) of the FE model and the selected ROM.

The nonlinear restoring forces are plotted to identify the nonlinear characteristics of the system. To this end, nonlinear transient analyses are performed in ANSYS. For the sake of brevity, only the nonlinear restoring force associated with the

[1] the mass of the beams is considered for 1/3

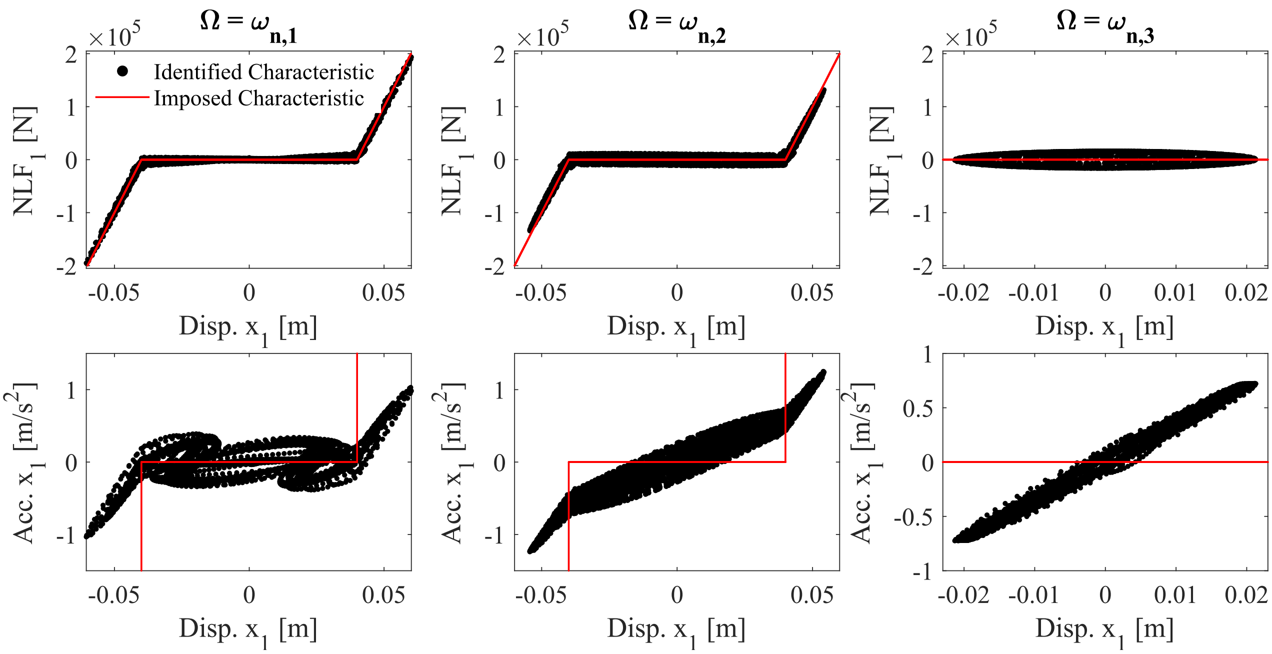

Fig. 4 Lateral view of the identified linear/nonlinear restoring force surfaces (black dots) and associated nonlinear characteristics imposed in ANSYS (red line). The panels in the top row show the nonlinear restoring force surfaces of the first DOF as defined in Eq. 5a, while the bottom panels shows the results obtained with the classical restoring force surface method. From left to right, the panels in the first, second, and third column shows the results obtained using the transient response of the system when, respectively, the first, second, and third natural frequency are used as excitation source.

first DOF of the structure are plotted, for three different excitation frequencies, namely the three natural frequencies $\omega_{n,1}$, $\omega_{n,2}$, and $\omega_{n,3}$. The nonlinear analysis shows that, when the excitation frequency Ω is equal to the first ($\omega_{n,1}$) or the second ($\omega_{n,2}$) natural frequency of the system, contact between the first storey and the limit motion constraint occurs; instead, when the frequency of excitation is increased and matches $\omega_{n,3}$ no contact occurs in the system. At this stage it is possible to plot the nonlinear restoring forces in a subspace of coordinate which is chosen to be x_1 and $\dot{x}_1$. The results are reported in Fig. 4 where the later view of surface (black dots) is shown and compared against the characteristic to be identified (red line). In order to make a comparison with the classical restoring force surface method the acceleration of the mass, typically used in base excited structures (see for example [11]), is plotted in the second row of Fig. 4. The results demonstrates that at the first two excitation levels (i.e. $\Omega = \omega_{n,1}$ and $\Omega = \omega_{n,2}$), the NLRF surface is able to reconstruct the nonlinear piecewise characteristic applied to the system. When the excitation Ω is equalt to $\omega_{n,3}$ contact does not occur and thus the NLRF surface shows a flat line close to zero. On the contrary, the classical approach perceives the present of non-smooth characteristic but it does not allow the accurate identification of the nonlinearity. In addition, the presence of the linear contributions associated to all the DOFs of the system, leads to the generation of an hypersurface rather than simple 3D surface. This concept is clearly highlighted by Fig. 5 where the surfaces associated to $\Omega = \omega_{n,1}$ are plotted in isometric view.

Experimental Validation: Identification of Smooth and Non-Smooth Nonlinearities

The proposed method is utilised to identify the nonlinear characteristics of two similar test-rigs: the first test rig is characterised by smooth geometric nonlinearities while the second one presents an additional localised non-smooth characteristic. The two test rigs are shown in Fig. 6: the first test rig (left panel of Fig. 6) is mounted on a vibrating table whose amplitude is controlled by a feedback sensor (optical laser). The second test rig (right panel of Fig. 6), instead, is excited by the motion of single support whose motion is controlled by the voltage that is imposed on the shaker. Firstly, the linear dynamic behaviour of the two experimental model need to be identified. In this paper, the NLRF method is utilised to identify the full nonlinear behaviour of the first test rig and the the localised nonlinearity of the second test rig. This affect the definition of the ROMs that are used to identify the sought nonlinear characteristics.

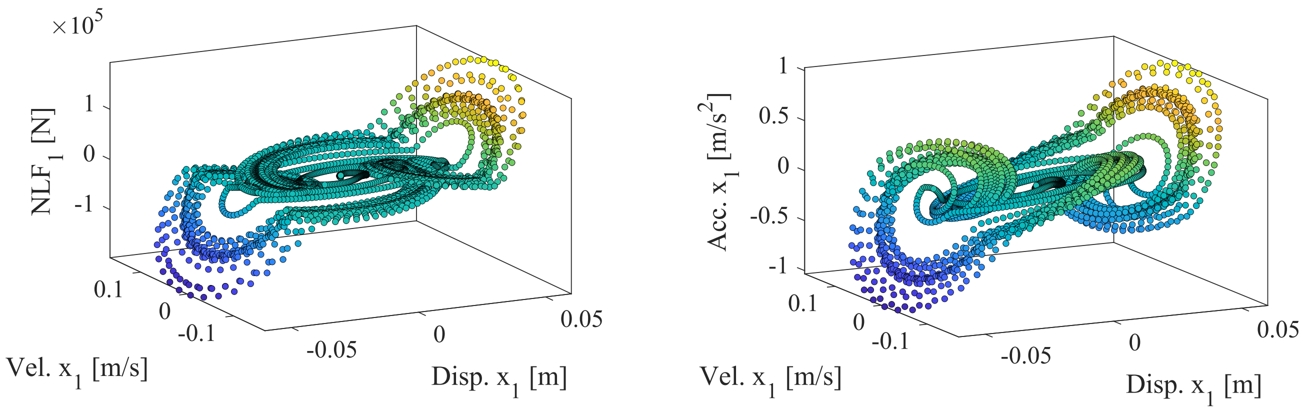

Fig. 5 Isometric view of the identified linear/nonlinear restoring force surfaces. The panel on the left represents the nonlinear restoring force surface while the panel on the right shows the classical representation of the restoring force surface for base-excited systems.

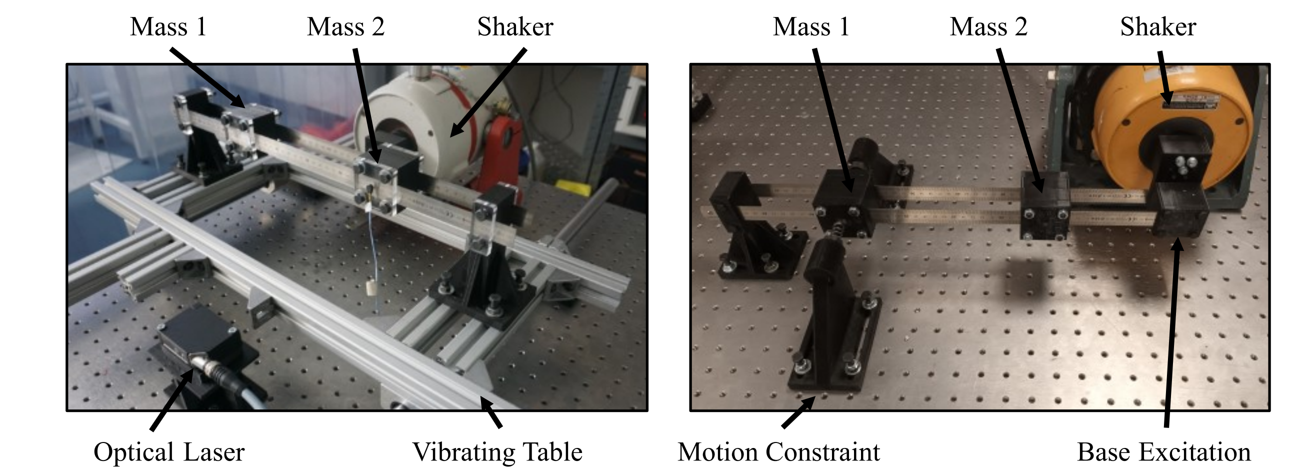

Fig. 6 Experimental test rigs: two-mass system characterised by smooth (left panel) and non-smooth (right panel) nonlinearities. The first experimental model is excited by a vibrating table while the second one is excited by the motion of single support.

The linear behaviour of the first test rig is identified using a two-DOF model which is described by the following set of ODEs:

$$m\ddot{z}_1 + c_1\dot{z}_1 + c_2(\dot{z}_1 - \dot{z}_2) + k_1 z_1 + k_2(z_1 - z_2) + NLF_1(z_1, z_2, \dot{z}_1, \dot{z}_2) = -m\ddot{y} \tag{6a}$$

$$m\ddot{z}_2 + c_3\dot{z}_2 - c_2(\dot{z}_1 - \dot{z}_2) + k_3 z_2 - k_2(z_1 - z_2) + NLF_2(z_1, z_2, \dot{z}_1, \dot{z}_2) = -m\ddot{y} \tag{6b}$$

where y represents the base displacement, $z = x - y$ indicates the relative displacement between the base and the masses, and NLF_1 and NLF_2 are the nonlinear restoring terms associated with the first and second DOF of the model. The linear coefficients are identified via circle fitting method and are reported in Tab. 1. The interested reader can find additional details about the identification of the underlying linear system of the first test rig at the following reference [15].

The linear and nonlinear smooth behaviour of the second test rig is described by the following ROM:

$$m\ddot{x}_1 + c_1\dot{x}_1 + k_1 x_1 + c_2(\dot{x}_1 - \dot{x}_2) + k_2(x_1 - x_2) + \mu_1 x_1^3 + \mu_2 x_1^3 - \mu_{2,b} x_1^2 x_2 + \mu_{2,b} x_1 x_2^2 - \mu_2 x_2^3 + NLF_1 = 0 \tag{7a}$$

$$m\ddot{x}_2 + c_3(\dot{x}_2 - \dot{y}) + k_3(x_2 - y) - c_2(\dot{x}_1 - \dot{x}_2) - k_2(x_1 - x_2) + \mu_3(x_2 - y)^3 - \mu_2 x_1^3 + \mu_{2,b} x_1^2 x_2 - \mu_{2,b} x_1 x_2^2 + \mu_2 x_2^3 = 0 \tag{7b}$$

where x represents the absolute displacement of the two masses, y indicates the base displacement, k_1, k_2, and k_3 are the linear stiffness coefficients, c_1, c_2, and c_3 denote the linear damping coefficients, and μ_1, μ_2, $\mu_{2,b}$, and μ_3 are the nonlinear stiffness coefficients. This ROM has been identified and validated in [18] and this information are utilised to identify localised nonlinearities in the second test rig, using the proposed method. The linear parameters of the system are once again identified via circle fitting method and are reported in Tab. 1. The remaining smooth nonlinear parameters have been identified via meta-heuristic optimisation and, for completeness, are reported in Tab. 2. Details of the identification and validation procedures can be found at the following references [18, 16].

At this stage it is possible to proceed with the identification of the nonlinear characteristics of both rest rigs. Firstly, the NLRF surfaces must be plotted in a reduced sub-space of coordinates: the results are reported in Fig. 7 where the NLRF surfaces of the first DOF for the first and second test rig are shown. It is worth mentioning, that the two test rigs are excited via sinusoidal frequency sweeps in two different ways: the vibrating table of the first test rig is controlled in amplitude via closed-loop control. This allows imposing a certain amplitude of the base excitation. On the contrary, the second test rig does not present a closed-loop control, and frequency sweeps across the first two linear resonances are performed by imposing the amplitude of the sinusoidal voltage signal the is passed to the shaker. Further details about the experimental analysis of the two test rigs can be found in [19, 15].

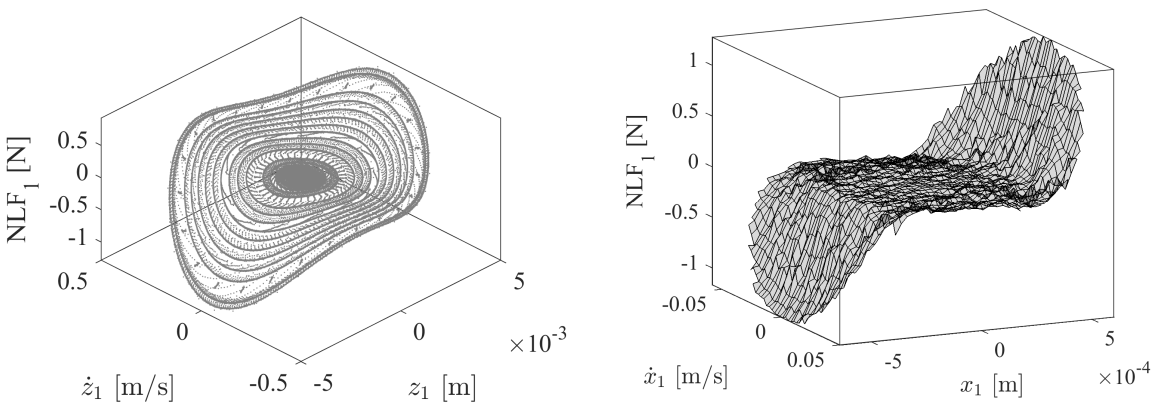

Fig. 7 Experimental NLRF surfaces of the first test rig (left panel) and second test rig (right panel). The surfaces are obtained by imposing, respectively, a base amplitude of 0.05 mm and voltage input of 0.3 V. The coordinates of the first DOF, i.e. $z_1 - \dot{z}_1$ and $x_1 - \dot{x}_1$, are used to plot the NLRF surfaces associated with the first DOF of the selected ROM.

In both cases, the coordinates of the local DOF, e.g. x_1 and $\dot{x}_1$ for the first DOF, are used as reduced sub-space to plot the surfaces. The NLRF surface of the first test rig considers all the nonlinear dynamics of the system and it can be represented as a 3D function in the considered sub-space of coordinates. Similarly the NLRF surface of the second DOF of the first test rig (here not represented) shows the same property. This result is suggesting that the selected coordinates, i.e. $z_1 - \dot{z}_1$ for the first DOF and $z_2 - \dot{z}_2$ for the sscond DOF, are sufficient to describe the nonlinear characteristics of the first test rigs. This information is then utilised to mathematically model the sought nonlinear characteristic which results in the following expression:

$$\begin{cases} NLF_1 = a_1 z_1^2 + a_2 z_1 \dot{z}_1 + a_3 \dot{z}_1^2 + a_4 z_1^3 + a_5 \dot{z}_1^3 + a_6 z_1 \dot{z}_1^2 + a_7 z_1^2 \dot{z}_1; \\ NLF_2 = b_1 z_2^2 + b_2 z_2 \dot{z}_2 + b_3 \dot{z}_2^2 + b_4 z_2^3 + b_5 \dot{z}_2^5; \end{cases} \tag{8}$$

Eq. 8 represents the form of the nonlinear characteristic of the first test rigs and its polynomial degree can be obtain thorugh the iterative procedure described in [15].

Table 1 Linear coefficients identified from the experimental linear transfer functions in Ref. [16, 15]. The first line indicates linear coefficients of the first test rig while the second line shown the linear coefficients identified from the experimental data of the second test rig.

Coefficients	m [kg]	c_1 [Ns/m]	c_2 [Ns/m]	c_3 [Ns/m]	k_1 [N/m]	k_2 [N/m]	k_3 [N/m]
Test rig 1	0.1130	0.0582	0.0205	0.0600	1232.9	225.1	1261.9
Test rig 2	0.1365	0.0454	0.0075	0.0366	714.9	89.6	624.9

Table 2 Nonlinear smooth parameters identified in [18]. The parameters are identified via meta-heuristic optimisation.

μ_1 [N/m^3]	μ_2 [N/m^3]	$\mu_{2,b}$ [N/m^3]	μ_3 [N/m^3]
2.732e+06	1.324e+06	8.850e+06	7.069e+06

Similarly, from inspection of the NLRF surface of the second test rig, a nonlinear function representing the type of nonlinearity is identified of the second experimental model. In this case, a piecewise function is considered to be a valid representation of the nonlinearity. The sought nonlinear characteristic is mathematically represented by the following expression:

$$NLF = \begin{cases} k_p(x_1 - a_2) & \text{if } x_1 > a_2 \\ 0 & \text{if } -a_1 < x_1 < a_2 \\ k_p(x_1 + a_1) & \text{if } x_1 < -a_1 \end{cases} \tag{9}$$

where k_p is the piecewise stiffness and, a_1 and a_2 are the lower and upper limits of the semi free-play gap. At this stage, it is possible to identify the unknown coefficients by imposing and solving a minimisation problem. The results are reported in Tab. 3 for the first test rig and in Tab. 4 for the second test rig.

Table 3 Experimental nonlinear coefficients, identified from the nonlinear restoring force surfaces in [15].

Monomial (M_1)	Coefficient	Value	Monomial (M_2)	Coefficient	Value
z_1^2	a_1	$-8.4608 \times 10^3\,\mathrm{N/m^2}$	z_2^2	b_1	$-8.3989 \times 10^3\,\mathrm{N/m^2}$
$z_1\dot{z}_1$	a_2	$5.3189\,\mathrm{Ns/m^2}$	$z_2\dot{z}_2$	b_2	$-4.8546\,\mathrm{Ns/m^2}$
$\dot{z}_1^2$	a_3	$0.9055\,\mathrm{Ns^2/m^2}$	$\dot{z}_2^2$	b_3	$0.9047\,\mathrm{Ns^2/m^2}$
z_1^3	a_4	$1.1237 \times 10^7\,\mathrm{N/m^3}$	z_2^3	b_4	$1.1231 \times 10^7\,\mathrm{N/m^3}$
$\dot{z}_1^3$	a_5	$1.9777\,\mathrm{Ns^3/m^3}$	$\dot{z}_2^5$	b_5	$-8.0214\,\mathrm{Ns^5/m^5}$
$z_1\dot{z}_1^2$	a_6	$-1.3876 \times 10^2\,\mathrm{Ns^2/m^3}$	–	–	–
$z_1^2\dot{z}_1$	a_7	$1.0495 \times 10^4\,\mathrm{Ns/m^3}$	–	–	–

Table 4 Parameters of the piecewise function identified in [16].

a_1 [m]	a_2 [m]	k_p [N/m]
4.091×10^{-4}	3.995×10^{-4}	5.472×10^3

Once the nonlinear characteristics are identified, the dynamics of the numerical models and experimental test rigs are compared. The comparison is carried out using dynamic responses of the experimental test rigs that were not used during the identification procedure: specifically, the NLRF surfaces of the first and second test rigs were obtained by imposing an amplitude of excitation of, respectively, 0.05 mm and 0.3 V. The dynamics of the first test rig is investigated also at amplitude of the vibration table equal to 0.04 mm and 0.03 mm; these additional data are utilised to carry out the comparison between the numerical and experimental FRCs in the case of the first test rig. The first numerical model is solved using the toolbox COCO [20] via numerical continuation and the results are reported in Fig. 8 where the FRCs are shown in terms of amplitude of the first DOF. The figure shows that the numerical model is able to capture the dynamics of the experimental test rig in terms of amplitude of response and jumps from high to low amplitude solution, even when the experimental and numerical models are compared in excitation conditions that are different from the one utilised during the identification phase. The results of Fig. 8 are satisfactory in terms of prediction capabilities of the model therefore the identified numerical model is considered to be validated.

A similar validation procedures is repeated for the numerical model representing the second test rig: in this case, time-histories and phase-portraits at different frequencies of excitation are used to carry the comparison. This choice is motivated by the very rich and complicate dynamic response of this class system which include grazing bifurcations, multi-periodic isolas, quasi-periodic responses, and chaos. The reader interested in the numerical and experimental dynamics of this class of system is invited to read the following references [19, 21]. The NLRF surface of the second test rig is obtained using data associated to an amplitude of excitation of 0.3 V. The test rigs is also tested using a voltage input of 0.35 V, thus the dynamics responses associated to this condition are utilised to carry out the validation process. Specifically the following conditions are considered: a single period attractor, identified at 11.9 Hz, and a multi-periodic attractor, found when the excitation frequency is equal to 12.1 Hz. The results of the comparison are shown in Fig. 9 where it is demonstrated that the identified nonlinear model is able to capture the dynamics of the experimental test rig from a quantitative and qualitative

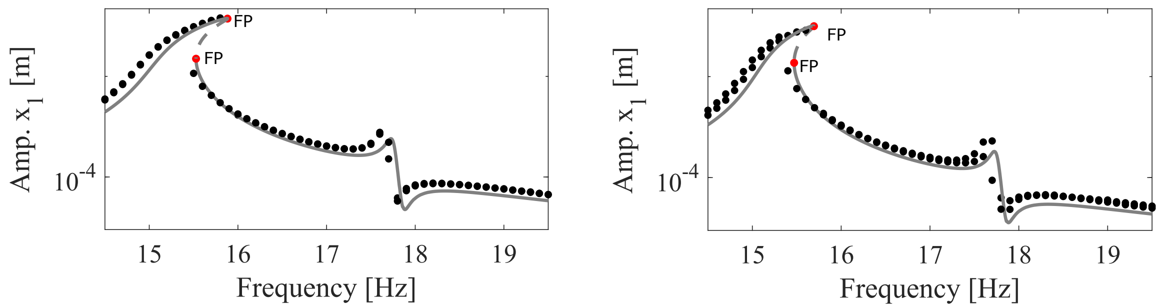

Fig. 8 Comparison between experimental (dots) and numerical FRC (continuous line) in terms of amplitude of the first DOF. The panel on the left shows the comparison between FRCs when an amplitude of excitation equal 0.04 mm is utilised. The panel on the right shows the same comparison when an amplitude of 0.03 mm is imposed to the base.

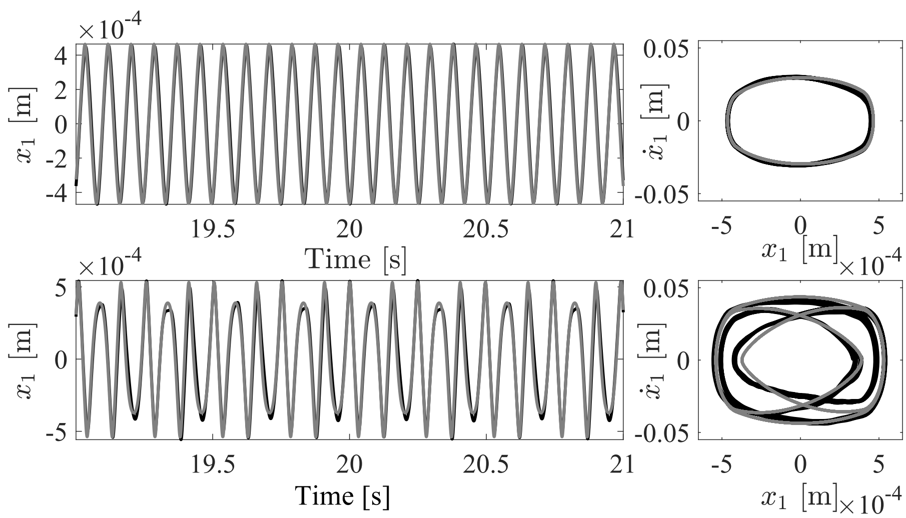

Fig. 9 Comparison between experimental (black continuous line) and numerical results (gray continuous line). The panels on the left show the time-histories while the panels on the right show the orbits. Different attractors are considered, namely, a single period attractor at 0.35 V (panels in the top row) and multiperiodic attractor at 0.35 V (panels in the bottom row).

point of view, in term of time histories and type of attractor. These results confirms the prediction capability of the identified model which is considered to be validated.

Conclusions

This paper presented an overview of novel identification method named the Nonlinear Restoring Force (NLRF) method. The method builds on the separation of linear and nonlinear components of the restoring force, allowing to be interfaced with the current model identification practices utilised in industry. By obtaining a graphical representation of the pure nonlinear response in a reduced sub-space of coordinates, the user can obtain additional insights on the nonlinear dynamics of the system. This enables a quick and easy identification of localised nonlinearities and helps to understand if the selected set of coordinates can fully describe the nonlinear restoring force of the system.

Firstly, the mathematical background, the methodology, and the limitations of the proposed method are presented. Then a numerical example of a nonlinear three storeys building is proposed. To this end, a numerical FE model of the building is created and Ansys and it is utilised to obtain the dynamic response of the structure. Then the NLRF method is utilised to reconstruct the nonlinear restoring force surfaces and identify the nonlinearity. The NFRM method is then used to identify the nonlinear characteristics of two experimental test rigs characterised by smooth and non-smooth nonlinearities. Once again, the NLRF surfaces are obtained using the proposed methodology, identifying the associated nonlinear characteristics. The identified models are then validated against experimental data; to this end, experimental dynamic responses at different amplitudes of excitation are used. Specifically, the validation process is done using data associated to excitation conditions that were not used during the identification process. This guarantees an higher degree of reliability of the identified model, especially outside the ranges of experimental analysis. The comparison shows that the identified numerical models are able capture the dynamics of the experimental test rigs under several excitation conditions, thus validating and concluding the study.

Data Availability

The experimental data utilised in this paper are available at the following DOI [22, 23].

Acknowledgments The authors would like to acknowledge the following NERC and EPSRC grants: GALLANT, Glasgow as a Living Lab Accelerating Novel Transformation (No. NE/W005042/1), RELIANT, Risk EvaLuatIon fAst iNtelligent Tool for COVID19 (No. EP/V036777/1).

References

1. F.A. Prince. "Weight and the future of space flight hardware cost modeling". In *International Society of Parametric Analysis/Society of Cost Estimating and Analysis 2003 International Conference*, 2003.
2. R.N. Yancey. *Challenges, opportunities, and perspectives on lightweight composite structures: aerospace versus automotive.* Lightweight composite structures in transport (2016): 35-52.DOI: https://doi.org/10.1016/B978-1-78242-325-6.00002-5
3. Official Journal of the European Union. *The European Green Deal*. European Parliament, 2020.
4. Department of Energy & Climate Change. *The UK Low Carbon Transition Plan*. Government of the United Kingdom, 2009.
5. M. Friswell, and J.E. Mottershead, *Finite element model updating in structural dynamics.* Springer Dordrecht, 1995. DOI: https://doi.org/10.1007/978-94-015-8508-8
6. D.J. Ewins. *Modal testing: theory, practice and application*. John Wiley & Sons, 2009.
7. G. Kerschen, K. Worden, A.F. Vakakis, and J.C. Golinval. "Past, present and future of nonlinear system identification in structural dynamics". *Mechanical System and Signal Processing*, 20:505–592, 2006. DOI: https://doi.org/10.1016/j.ymssp.2005.04.008
8. J.P. Noël and G. Kerschen. "Nonlinear system identification in structural dynamics: 10 more years of progress". *Mechanical Systems and Signal Processing*, 83:2–35, 1 2017. DOI: https://doi.org/10.1016/j.ymssp.2016.07.020
9. S.F. Masri and T.K. Caughey. "A nonparametric identification technique for nonlinear dynamic problems". *Journal of Applied Mechanics*, 46:433–447, 1979. DOI: https://doi.org/10.1115/1.3424568
10. E. Bonisoli and A. Vigliani. "Identification techniques applied to a passive elasto-magnetic suspension". *Mechanical Systems and Signal Processing*, 21:1479–1488, 4 2007. DOI: https://doi.org/10.1016/j.ymssp.2006.05.009
11. A. Cammarano, S. G. Burrow, and D. A.W. Barton. "Modelling and experimental characterization of an energy harvester with bi-stable compliance characteristics". *Proceedings of the Institution of Mechanical Engineers. Part I: Journal of Systems and Control Engineering*, 225:475–484, 6 2011. DOI: https://doi.org/10.1177/0959651811403093
12. G. Kerschen, M. Peeters, J.C. Golinval, and C. Stéphan. "Nonlinear modal analysis of a full-scale aircraft". *Journal of Aircraft*, 50:1409–1419, 2013. DOI: https://doi.org/10.2514/1.C031918
13. J.P. Noël, L. Renson, and G. Kerschen. "Complex dynamics of a nonlinear aerospace structure: Experimental identification and modal interactions". *Journal of Sound and Vibration*, 333:2588–2607, 2014. DOI: https://doi.org/10.1016/j.jsv.2014.01.024
14. S.F. Masri, F. Tasbihgoo, J.P. Caffrey, A.W. Smyth, and A. G. Chassiakos. "Data-based model-free representation of complex hysteretic mdof systems". *Structural Control and Health Monitoring*, 13:365–387, 1 2006. DOI: https://doi.org/10.1002/stc.147
15. C. Martinelli, A. Coraddu, and A. Cammarano. "Strongly nonlinear multi-degree of freedom systems: Experimental analysis and model identification". *Mechanical Systems and Signal Processing*, 218:111532, 2024. DOI: https://doi.org/10.1016/j.ymssp.2024.111532
16. C. Martinelli, A. Coraddu, and A. Cammarano. "Identifying localised nonlinearities: Nonlinear restoring force surface in piecewise multi-degree-of-freedom systems". In *Society for Experimental Mechanics Annual Conference and Exposition*. pages 19-26. Springer, 2024, DOI: https://doi.org/10.1007/978-3-031-69409-7_4
17. K. Worden, and G.R. Tomlinson. *Nonlinearity in structural dynamics: detection, identification and modelling*. CRC Press, 2001.
18. C. Martinelli, A. Coraddu, and A. Cammarano. "Experimental parameter identification of nonlinear mechanical systems via meta-heuristic optimisation methods". In *Society for Experimental Mechanics Annual Conference and Exposition*, pages 215–223. Springer, 2023. DOI: https://doi.org/10.1007/978-3-031-36999-5_28
19. C. Martinelli, A. Coraddu, and A. Cammarano. "Experimental analysis of a nonlinear piecewise multi-degrees of freedom system". In *International Conference on Nonlinear Dynamics and Applications,* pages 665-675. Springer International Publishing, 2023, DOI: https://doi.org/10.1007/978-3-031-50631-4_56
20. H. Dankowicz and F. Schilder. "Recipes for continuation". *SIAM*, 2013.
21. C. Martinelli, A. Coraddu, and A. Cammarano. "Approximating piecewise nonlinearities in dynamic systems with sigmoid functions: advantages and limitations". *Nonlinear Dynamics*, 111, 8545–8569, 2023. DOI: https://doi.org/10.1007/s11071-023-08293-1
22. C. Martinelli, A. Coraddu, and A. Cammarano. "Strongly nonlinear multi-degree of freedom systems: Experimental analysis and model identification [data collection]". *Enlighten Research Data*, 2023. DOI: 10.5525/gla.researchdata.1621
23. C. Martinelli, A. Coraddu, and A. Cammarano. "Experimental analysis of a nonlinear piecewise multi-degrees of freedom system [data collection]". *Enlighten Research Data*, 2023. DOI: 10.5525/gla.researchdata.1471